SEPARATING THE EFFECTS OF WALL-BLOCKING AND NEAR-WALL SHEAR IN THE INTERACTION BETWEEN THE WALL AND THE FREE-SHEAR LAYER IN A WALL JET

A. Dejoan and M. A. Leschziner
Department of Aeronautics, Imperial College London,
London SW7 2AZ, United Kingdom
a.dejoan@imperial.ac.uk, mike.leschziner@imperial.ac.uk

ABSTRACT

The statistical characteristics of two plane jets, one developing along a real wall and the other along a frictionless wall (equivalent to a zero-shear, non-deformable free surface) are compared by way of highly-resolved LES solutions at computational conditions close to DNS. The aim is to distinguish between two types of interaction of the outer shear layer with the wall: one inviscid, arising from wall blocking, and the other, associated with the near-wall shear in the boundary layer. Results are presented for mean-flow properties, second moments and budgets thereof, and for integral length scale. The comparisons demonstrate that, while the boundary layer adds distinctive features to the near-wall region, associated with turbulence production redistribution and small-scale activity, the outer shear layer and its inviscid interaction with the wall are the dominant features. The effect of the outer layer, in particular the high level of diffusion of turbulence towards the wall, renders the boundary layer very different from a conventional near-wall shear layer.

INTRODUCTION

The processes by which a free shear layer — say, one that evolves following separation — interacts with a near-wall layer adjacent to it across an "overlap" region can have a significant impact on the gross behaviour of the flow containing these shear layers. Examples in which such an interaction occurs are separated flows recovering from reattachment, wall jets injected into or across an ambient flow in the context of wall cooling, heating and separation control, and impinging jets used to enhance heat transfer or arising in VSTOL aircraft operation.

From a fundamental point of view, the interaction can lead to a substantial modification of both component flows, for example, by the penetration or "migration" of disparate turbulent scales from one shear layer to the other. This process can have significant implications to the rate of mixing of the flow as a whole and the turbulence structure within it. It is important, therefore, to understand the fundamental mechanisms involved, both as an end in itself and as a foundation for developing improved statistical closures for such flows. Modelling post-reattachment recovery is a case in point: it is often observed that turbulence closures that predict correctly the separated zone, including the reattachment point, underestimate the rate of recovery. In this region, the turbulence structure of the flow departs substantially from the equilibrium conditions that are used to formulate and calibrate models for near-wall shear flows. This lack of equilibrium is not merely due to upstream history, but also linked to cross-stream transport that is driven by the disparity of the constituent layers that form the post-reattachment wake.

A generic model flow that features the type of interactions considered above is the (statistically) two-dimensional wall jet. This consists of an outer, separated shear layer and an inner boundary layer which "communicate" across an "overlap" region. Recent highly-resolved LES studies by the present authors (Dejoan and Leschziner, 2004a, 2004b) have highlighted some influential mechanisms specific to the interaction between the two shear layers - in particular, the influence of turbulent-stress diffusion across the overlap region and the migration of large-scale eddies from the outer to the inner flow. Taking advantage of the data generated for the wall jet, a recent paper by the present authors (Dejoan and Leschziner, 2005) investigates, by way of *a-priori* studies as well as model calculations, the validity of the second-moment-closure approximations for the wall jet, and demonstrates a rather poor representation of stress diffusion and pressure-velocity interaction.

An interesting question that arises when studying the wall jet, or any other wall-affected set of shear layers, is what the relative contributions of near-wall shear and the inviscid wall-blocking are to the observed interaction across the overlap region. In the context of statistical modelling, this question is of interest in efforts to devise improved second-moment-closure models, particularly in the case of models in which the anisotropy due to shear and wall-blocking are approximated by separate closure fragments. The two contributions may be investigated by comparing the flow in a realistic wall jet with one in which the wall is treated as being shear-free - essentially, a non-deforming free surface. While in both flows, wall-blocking causes wall-normal fluctuations to decline, an obvious difference is that the tangential fluctuations decay to zero only in the presence of the real wall (and hence shear). Another difference is that the absence of wall shear prevents the generation of near-wall turbulence that has structure and scales peculiar to such conditions and distinct from those is the outer shear layer. Hence, the interaction between the outer layer and the near-wall region is expected to be different in the two flows. This is the subject that is addressed in the present paper. Thus, statistics derived from highly-resolved simulations for the flows are juxtaposed, including budgets, in an effort to highlight any important differences in the interaction that arise when wall-shear is added to wall-blocking.

THE FLOWS AND THE APPROACH TO THEIR SIMULATION

In both geometries, the jet is injected at the velocity U_o through a slot of height b in a vertical wall (see Fig. 1). The Reynolds number, $R_e = U_o b/\nu$, is 9600. The size of the domain is $22b \times 10b \times 5.5b$ in the streamwise, transverse and spanwise directions, respectively. The choice of this configuration is based on experimental observations by Eriksson *et al.* (1998) for the same conditions as simulated here (with the no-slip state imposed at the wall), indicating that the flow essentially reaches a self-similar state at 20 jet heights. At the inflow, $x/b = 0$, the time-mean velocity and turbulence-intensity profiles have been extracted from the experimental conditions. The inlet flow is effectively laminar, with the measured low level of fluctuations therein represented by superposing weak random perturbations onto the mean inlet flow. At the outflow, $x/b = 22$, a non-reflective, convective boundary condition is applied. At the upper ("entrainment") boundary, $y/b = 10$, a theoretically determined distribution of entrainment velocity not exceeding 5% of the velocity U_o is prescribed. At the lower boundary, impermeability and no-slip condition are applied for the wall jet, while the zero-shear wall conditions, $V = 0$ and $\partial U/\partial y = \partial W/\partial y = 0$) are imposed for the equivalent "free-surface" jet. The numerical grid contains 420x208x96 (8.4 million) nodes, and has been carefully chosen so as to give very low subgrid-scale contributions, approximated with Germano's dynamic Smagorinsky model (Germano *et al.*, 1991). Fig. 2 shows the ratio of cell size, Δ, to the Kolmogorov length, $\eta = \nu^{3/4}\varepsilon^{-1/4}$ (where ε is the dissipation), to be, typically, 5-10. These distributions were determined using data for the rate of dissipation derived from the balance of all other contributions to the turbulence-energy budget. Consistent with the above are the observations that the time-mean subgrid-scale viscosity is of the order 0.5 times the fluid viscosity, and that the dissipation rate extracted explicitly from the simulation is about 70% of that determined from the balance. Moreover, the spectra shown in Fig. 3 demonstrate the cut-off to lie in the dissipative range. In the outer shear-layer, the wall-normal grid distance ranges from $\Delta y/b = 0.02$ to 0.05 in the region $1 < y/b < 5$. In the wall shear-layer, the region $0 < y/b < 1$ is covered by 100 nodes. In the wall jet, the near-wall cell-aspect ratio is, typically, $\Delta y^+/\Delta x^+/\Delta z^+ = 1.2/24/24$, the wall-nearest grid node lying at $y^+ = 0.6$. Statistical results, presented in the next section, were obtained by integration over 20 and 26 flow-through times for the real and shear-free-wall jets, respectively, the longer integration time of the latter necessitated by the more pronounced presence and persistence of long-time-scales eddies in the outer part of the shear layer. The computational method is a general multiblock finite-volume scheme incorporating second-order discretisation in time and space. Time-marching is based on a fractional-step and projection method. The code is fully parallelised and was run on up to 512 ORIGIN 3800 processors. More details on the simulation parameters can be found in Dejoan and Leschziner (2004a).

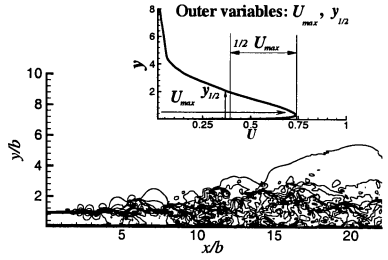

Figure 1: Wall-jet geometry.

RESULTS

Introductory considerations

When examining the wall jet on its own, by reference to measurements of Eriksson *et al.* (1998), Dejoan and Leschziner (2004a, 2004b) present comparisons in inner, outer and mixed scaling. Here, comparisons are only possible in terms of quantities normalised by the outer scales U_{max} and $y_{1/2}$, the distance from the wall to the half-of-maximum-velocity point (see Fig. 1). With this scaling, the outer layers in both flows considered exhibit a self-similar behaviour far downstream of the inlet. Thus, comparisons between the two flows can be made, at least in the outer layer, without reference to streamwise evolution of the flows. In what follows below, profiles of mean and turbulence properties as well as budgets are given for the location $x/b = 20$, at which both flows are close to being in a self-similar state. Fig. 1 illustrates the streamwise evolution of the wall-shear jet through the iso-contours of an instantaneous velocity field in one spanwise plane. This shows that transition in the outer shear layer occurs at around x/b=2, while turbulence is observed to be fully established at location $x/b \sim 12$. A similar behaviour has been observed for the zero-wall-shear jet.

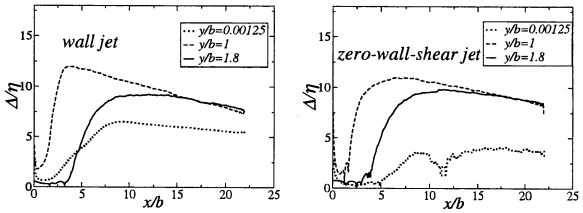

Figure 2: Ratio of the grid size to the Kolmogorov length scale given at different locations.

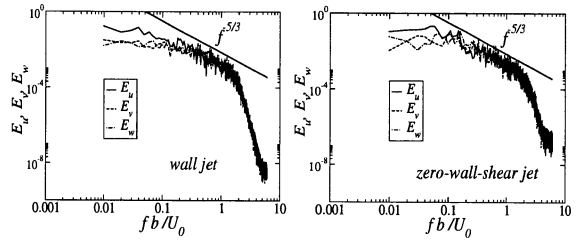

Figure 3: Frequency spectra given at $x/b = 20$, $y/b = 1$.

Mean-flow and turbulence properties

The mean-flow characteristics of the two jets are compared in Figs. 4 and 5 by way of distributions for the decay of maximum velocity, the spreading rate and mean-velocity components at $x/b = 20$. The comparisons show that the maximum streamwise velocity of the real wall jet decays faster an expected behaviour, because of the loss of momentum induced by the wall-shear stress. However, the spreading rates are close, that of the wall jet being slightly lower, $dy_{1/2}/dx = 0.073$, than the value for the zero-wall-shear jet, $dy_{1/2}/dx = 0.076$ (the linear extension of the spreading rate in Fig. 4 beyond the end of the computational domain $x/b = 22$ is intended to accentuate the difference).

The mean-velocity profiles, compared in Fig. 5, are fairly similar, except for U near the wall. One noteworthy difference is that the non-dimensional shear strain in the outer shear layer is lower in the absence of wall shear. This may be taken to suggest a higher level of cross-flow turbulent diffusion. Indeed, as will be shown below, the shear stress is higher in the wall-shear-free jet.

Comparisons of profiles of the Reynolds-stress components at $x/b = 20$ are given in Fig. 6. The most prominent differences between the two cases are, first, the finite value of the turbulence energy at the shear-free wall, and second, the sign reversal in the near-wall-shear stress in the real jet, associated with the sign reversal in the shear strain (the two reversals occur at different locations, however). The former is obviously a consequence of the impingement of the outer-layer turbulent motions on the wall, coupled with the absence of a viscous near-wall layer, which, in the real jet, fully damps the turbulent fluctuations at the wall. In the boundary layer, the three normal-stress components vanish, whereas, at the shear-free wall, only the wall-normal stress is damped. One important

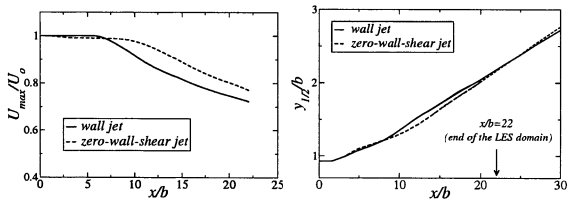

Figure 4: Left: decay of the maximum streamwise velocity. Right: spreading rate.

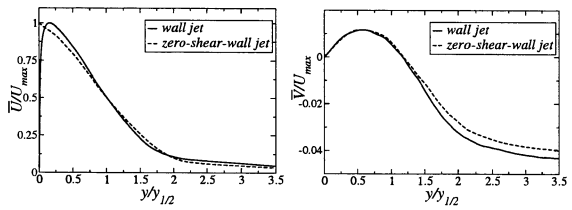

Figure 5: Mean streamwise and wall-normal velocity profiles at the location $x/b = 20$.

feature that differentiates the two flows is that, in the real jet, wall turbulence is generated by the high level of wall shear. This production process is directly associated with the near-wall peak in the streamwise stress, $\overline{uu}$. In contrast, the rise

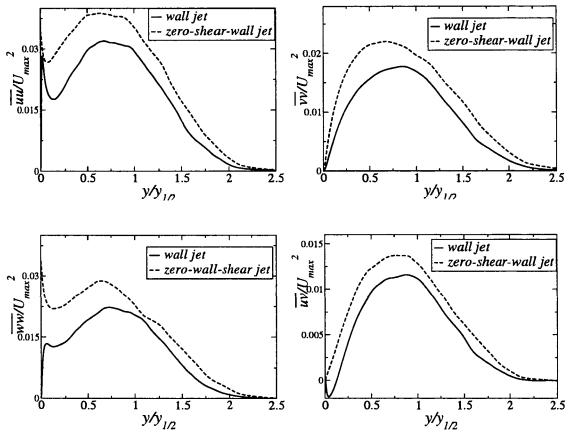

Figure 6: Profiles of Reynolds-stress components at the location $x/b = 20$.

in this stress in the absence of shear is, as will transpire from the budgets, a consequence of energy being transferred from $\overline{vv}$ to $\overline{uu}$ and $\overline{ww}$. The difference between the near-wall turbulence structure of the two flows is brought out well in Fig. 7. This shows clearly the streamwise streaks and fine elongated wall structures, which are characteristic of wall-shear flows. In contrast, in the absence of wall-shear, the near-wall structure is characterized by larger, more "isotropic" scales, as would be expected to form by the "splatting" of eddies without preferential wall-parallel orientation. It is this process that causes $\overline{uu}$ and $\overline{ww}$ to increase as the wall is approached, the stresses reaching almost identical maxima at the shear-free wall itself. This reflects a broadly symmetric redistribution of energy from the wall-normal stress component to the wall-parallel components by the velocity-pressure correlation. In the real jet, the inter-component energy transfer is also effective, but is different in character due to the wall-shear-induced turbulence production. In this case, the increase of the component $\overline{uu}$ due to the wall-shear is such that energy from $\overline{uu}$ has to be transferred to the spanwise component $\overline{ww}$. This redistribution process is associated with the minor near-wall peak of $\overline{ww}$. However, the intensity level of the spanwise stress $\overline{ww}$ is lower than $\overline{uu}$, reflecting a highly asymmetric redistribution of the turbulence energy in the wall-shear jet. A more detailed comparison, including an analysis based on the budgets terms involved in the redistribution of the turbulence energy is given in the next section.

A general conclusion derived from Fig. 6 is that, in absence of wall-shear, the turbulence activity is amplified, not only in the vicinity of the wall but also across the whole outer shear layer. This is a potentially important feature, for it suggests that effects arising from the viscous, sheared nature of the near-wall layers extend well beyond this layer, across the whole flow, possibly reflecting effects emanating from the substantial structural differences in the turbulence fields highlighted above. As will be shown later, the structural differences across the flow are also reflected by major differences in the integral length scale in the two flows.

Budgets

This section presents budgets for the turbulence energy and

the Reynolds-stress components extracted from the second-moment equations (1):

$$\underbrace{\frac{\partial \overline{u_i u_j}}{\partial t} + \underbrace{\overline{U}_k \overline{u_i u_j}_{,k}}_{C_{ij}}}_{\text{balance}=\varepsilon_{ij}} = \underbrace{\underbrace{-\overline{u_k u_j} U_{i,k} - \overline{u_k u_i} \overline{U}_{j,k}}_{P_{ij}} + \underbrace{\nu \overline{u_i u_j}_{,kk}}_{D_\nu} \underbrace{-\overline{u_i u_j u_k}_{,k}}_{TTT_{ij}} \underbrace{-\frac{(\overline{u_i p_{,j}} + \overline{u_j p_{,i}})}{\rho}}_{\Pi_{ij}} \underbrace{-2\nu \overline{u_{i,k} u_{j,k}}}_{\varepsilon_{c_{ij}}} + \text{SGS terms}}_{\text{balance}=\varepsilon_{ij}} \quad (1)$$

The budgets are presented in Figs. 8 to 12. Attention is confined to the near-wall region and to the region where the outer and inner layers strongly interact, which corresponds to $0 < y/y_{1/2} < 0.5$. The budgets pertaining to the outer region, beyond $y/y_{1/2} = 0.5$, are similar for the two flows and will be discussed elsewhere. The near-wall budgets, given in Figs. 8 to 12, show substantial differences between the two flows. The most important agency for these differences is the shear-induced generation at the wall, which directly affects k, $\overline{uu}$ and $\overline{uv}$. In the first two budgets, this production is compensated by a substantial elevation of dissipation, while in the case of the shear stress the increased (negative) production is compensated by a reversal of the pressure-velocity-interaction term from negative to positive. In the absence of wall shear, production is low (but not zero at the wall, because of a minor streamwise contribution). Hence, in the budgets of k and $\overline{uu}$ near-wall dissipation is also reduced. However, the reduction is also moderate and there is still a near-wall peak, but this is a result of increased diffusion towards the wall and an elevation of the pressure-velocity correlation. For $\overline{uu}$ (and as well for $\overline{ww}$, see below) the viscous diffusion becomes negative at the invisicd wall to balance, with dissipation, convection, turbulent diffusion and velocity-pressure correlation.

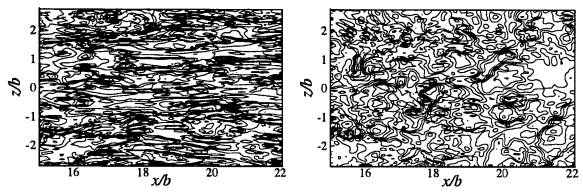

Figure 7: Instantaneous contours of the streamwise velocity in the streamwise/spanwise plane at $y/y_{1/2} \sim 0.02$. Left: real wall jet. Right: zero-wall-shear jet

The fact that the velocity-pressure correlation of $\overline{uu}$, negative in presence of wall-shear, exhibits a narrow positive peak very near the zero-shear wall and then becomes negative far away from the wall, implies a very different redistribution of energy between both flows: in the real jet, the component $\overline{uu}$ has to transfer energy to the other two components, while in absence of wall-shear $\overline{uu}$ receives energy in the very near-wall region and transfers energy away from the wall. More details on the mechanism of turbulence-energy redistribution will be given later.

One common feature shared by both flows is the importance of turbulent transport from the outer layer towards the wall, which reflects the strong interaction between the outer shear layer and the wall. This is especially prominent in the budgets of $\overline{vv}$. Although this stress is not dynamically active, it is of critical importance to the behaviour of $\overline{uv}$ and hence, indirectly, to that of the mean flow. The high level of diffusion is also noticeable in the budgets of $\overline{uv}$. In fact, in the presence of wall shear, this process is responsible of the displacement of the zero shear-stress and shear-strain positions and of a very limited log-low region (see Dejoan and Leschziner, 2004a). In absence of wall shear, shear-stress diffusion is high and compensated by negative velocity-pressure correlation. In contrast, in the presence of wall shear, the velocity-pressure correlation is forced to be positive to compensate, with the help of turbulent diffusion, the strong negative production.

A striking difference between the budgets of $\overline{vv}$ arises from the role of the velocity-pressure correlation. In both flows, production is virtually negligible and stress diffusion towards the wall from the outer shear-layer region is the dominant positive contributor close to the wall. In the presence of wall shear, the turbulent transport of $\overline{vv}$ is compensated mainly by dissipation and a slight negative near-wall peak of velocity-pressure correlation. This latter behaviour is not observed in a standard boundary layer, where turbulent transport is low and the velocity-pressure correlation is observed to be positive. The low (and negative) level of the velocity-pressure correlation is related to the high gain by turbulent transport. In absence of wall shear, this latter process appears to be amplified: the much higher input of stress diffusion is compensated by a much higher negative peak of the velocity-pressure correlation, with dissipation increasing only slightly. This suggests a different near-wall damping of the wall-normal stress between the two flows. In the near-wall region of the wall-shear-free jet, the peak of turbulent transport is higher and located closer to the wall. In presence of wall shear, turbulent transport is damped by viscous effects in the near wall region, which explains the lower level of velocity-pressure correlation. However, for both flows, the velocity-pressure correlation becomes positive for distances from the wall $y/y_{1/2} > 0.1$, indicating a reverse transfer of energy as the outer layer is approached.

One important feature to highlight, by reference to the zero-crossings of turbulent transport and the position of the peak diffusion, is the deeper penetration of the outer layer into the wall region when there is no wall-shear. This may be associated with the substantial structural differences in the near-wall turbulence of the two flows: in the absence of wall shear, the near-wall layer is populated with large-scale eddies which are more effective in transporting turbulence towards the wall.

As regards $\overline{ww}$, the budgets are similar, a main difference being the higher level of velocity-pressure correlation in presence of wall shear, reflecting a strong gain at the expense of the other stress components (see details below). Another difference is that, in absence of wall shear, convection is substantially higher, and this is associated with the higher near-wall level of $\overline{ww}$ combined with the maximum streamwise velocity at the inviscid wall. The dissipation of $\overline{ww}$ is not greatly affected by the presence of shear, except very close to the wall, where the stress has to be driven towards zero by viscous action.

As noted earlier, the role of the velocity-pressure correlation near the wall differs greatly between the two flows. To

gain further insight into this difference, profiles of the pressure-strain fragment, $\Phi_{ij} = \overline{p/\rho(u_{i,j} + u_{j,i})}$ for the normal stresses are compared for both flows on Fig. 13. Attention is drawn to the fact that the pressure-strain term, Φ_{ij}, differs from the pressure-velocity interaction Π_{ij} through the inclusion of pressure diffusion in the latter. In incompressible conditions, $\Phi_{kk} = 0$, and the pressure-strain acts purely as a redistributor of turbulence energy among the normal stresses. This figure brings to light more clearly the major effects of near-wall shear on the redistribution of energy related to velocity-pressure interaction processes. In presence of wall shear, in the near-wall region, energy is transferred from $\overline{vv}$ and from $\overline{uu}$ to $\overline{ww}$, whereas, in absence of shear, very close the wall, energy is transferred from $\overline{vv}$ to both $\overline{uu}$ and $\overline{ww}$. When wall shear is added, the component $\overline{uu}$ is mainly produced by shear strain, and this mechanism is so strong that energy has to be removed from $\overline{uu}$ to $\overline{ww}$. In absence of wall shear, the turbulent motions of the outer layer "splat" on the wall, and energy is transferred from the wall-normal stress to the wall-parallel components. Far away from the wall, as the outer layer is approached, the pressure-strain becomes negative for $\overline{uu}$ and positive for $\overline{vv}$ and $\overline{ww}$, indicating an energy transfer from the streamwise stress component to the wall-normal and spanwise component, a process which isotropizes the turbulence field and which is usually encountered in free shear flows. The pressure-strain of $\overline{vv}$ remains negative over a larger distance from the wall when wall shear is present. This suggests that $\overline{vv}$ starts to be damped further away from the wall, implying a more far-reaching influence of the wall on the outer layer and a higher level of anisotropy. This last point is also supported by the higher level of anisotropy in the dissipation rate in the presence of shear, as seen in the budgets of $\overline{uu}$, $\overline{vv}$ and $\overline{ww}$. Fig. 14 includes variations of the flatness parameter, $A = 1 - 9/8(A_2 - A_3)$, where $A_2 = a_{ij}a_{ij}$ and $A_3 = a_{ij}a_{jk}a_{kj}$ with $a_{ij} = \overline{u_i u_j}/k - 2/3\delta_{ij}$). This parameter is indicative of the level of anisotropy, in a scalar sense, varying between 1 for isotropic turbulence and 0 for two-component turbulence at the wall. In the context of modelling, A is of particular interest, for it is often used to procure the appropriate sensitivity of the pressure-strain approximation and dissipation equation to wall proximity. In both flows, A approaches zero in a broadly similar fashion. The steeper approach observed in the zero-wall-shear jet is related to the lower anisotropy of the stress field in the vicinity of the wall and, associated with it, the steeper decline of $\overline{vv}$ towards zero at the wall, seen in Fig. 6. One encouraging observation emerging from Fig. 13 is that A is well correlated with wall distance, regardless of whether or not the near-wall flow is sheared. On the other hand, the very different behaviour of Φ_{ij} (and also the anisotropy of the dissipation) calls into question as to whether A can be usefully exploited as the only parameter representing the effect of wall proximity in models for Φ_{ij} and ε_{ij}.

LENGTH SCALES

For the real wall jet, Dejoan and Leschziner (2004a) demonstrate, by reference to DNS results for channel-flow, that the length scale in the near-wall region is strongly elevated relative to the equilibrium level, reflecting the "migration" of large-scale eddies from the outer shear layer towards the wall. This is thus highlighted as one important aspect of the interaction between the outer shear layer and the wall layer. Here, Fig. 15 contrasts the integral length scale $k^{3/2}/\varepsilon$ of the real wall jet to the zero-wall-shear case. The major observation is that, in the absence of shear, the length scale experiences a further massive increase in the near-wall region. This increase therefore supports the notion of a wall-directed migration of eddies, referred to above. In the presence of shear, the boundary layer generates a range of scales which are considerably smaller - the difference being conveyed well in Fig. 7. These depress the integral scale as the wall is approached, reflecting an interpenetration of the two scale ranges. However, the influence of the outer-layer scales is very strong, and this causes the outer scale to substantially alter the boundary layer, right down to the wall, through the large input of turbulence energy by diffusion.

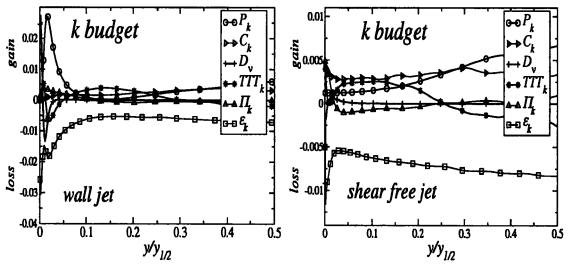

Figure 8: Budgets of the kinetic energy at the location $x/b = 20$. Normalised by $U^3_{max}/y_{1/2}$.

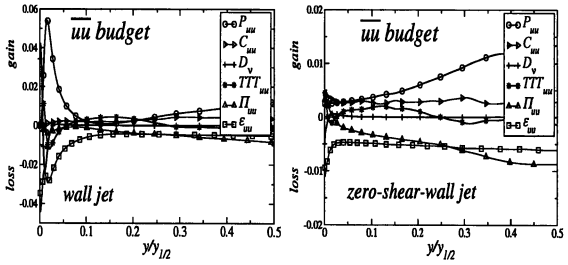

Figure 9: Budgets of the $\overline{uu}$ stress at the location $x/b = 20$. Normalised by $U^3_{max}/y_{1/2}$.

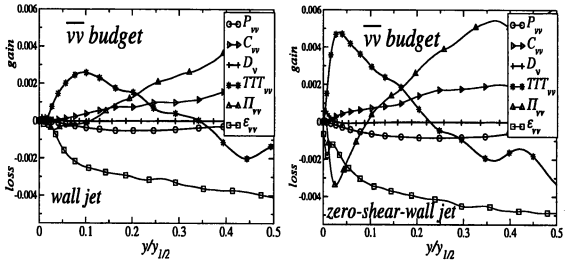

Figure 10: Budgets of the $\overline{vv}$ stress at the location $x/b = 20$. Normalised by $U^3_{max}/y_{1/2}$.

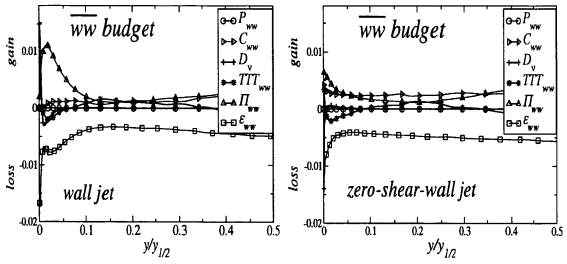

Figure 11: Budgets of the $\overline{ww}$ stress at the location $x/b = 20$. Normalised by $U^3_{max}/y_{1/2}$.

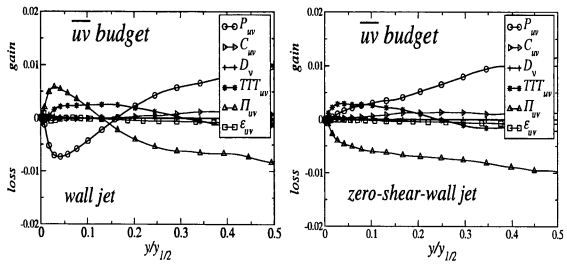

Figure 12: Budgets of the $\overline{uv}$ stress at the location $x/b = 20$. Normalised by $U^3_{max}/y_{1/2}$.

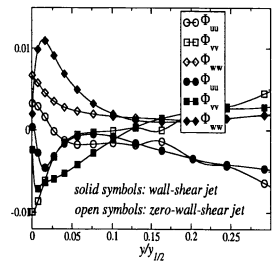

Figure 13: Pressure-strain profiles at the location $x/b = 20$. Normalised by $U^3_{max}/y_{1/2}$.

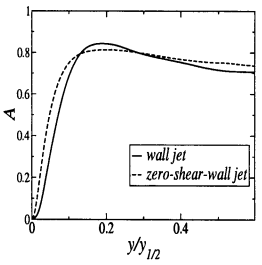

Figure 14: Flatness parameter profiles at the location $x/b = 20$.

CONCLUSIONS

The results presented here lead to the conclusion that, in absence of wall shear, the influence of the outer layer penetrates more deeply into the wall region and that the turbulence activity is enhanced not only in the near-wall region, but also across the whole outer layer. In presence of wall shear, the viscous effects damp the turbulence energy, not only in the layer close to the wall, but also well beyond. Both flows present very different structural properties in the near-wall region: fine and elongated streaks generated by the high wall shear contrast with much larger, more "isotropic" features in the absence of shear. Also, the integral length scale is found to be much higher in the absence of wall shear. Due to the presence of wall shear, a higher anisotropy of the stress field is observed in the real jet. In the zero-wall-shear jet, in the very near-wall

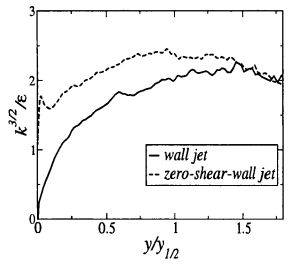

Figure 15: Integral length scale at the location $x/b = 20$.

region, a transfer of turbulence energy from the wall-normal stress component, $\overline{vv}$, to both wall-parallel components, $\overline{uu}$ and $\overline{ww}$, is effected. In the real jet, the energy redistribution is different: shear-produced energy has to be removed from $\overline{uu}$, so that the energy transfer is effected from $\overline{uu}$ and $\overline{vv}$ to $\overline{ww}$. Hence, the transfer of energy from $\overline{vv}$ to $\overline{uu}$, observed when only wall-blocking effects are present, is impeded by the presence of wall shear. One common feature of both flows is the importance of stress transported from the outer layer towards the wall. In particular, the budgets of $\overline{vv}$ show that the velocity-pressure correlation is very sensitive to the strong gain by stress diffusion and that, for the two flows, the velocity-pressure correlation acts, with dissipation, to remove the excess of $\overline{vv}$ carried by diffusion. In the zero-wall-shear jet, the latter process is accentuated, while in the real jet the process results in a budget of $\overline{vv}$ which differs substantially from that observed in a standard boundary layer. The differences observed in the redistribution of turbulence energy between the flows, coupled with the substantial contribution of turbulent transport in the near-wall region, pose a substantial challenge to the modelling of the pressure-velocity interaction in a wall region.

ACKNOWLEDGEMENTS

This sutdy was supported financially by the UK Science and Engineering Research Council (EPSRC). The computations were performed on the Origin 3800 computer at the national CSAR service in Manchester, using resources provided as part of the EPSRC grant.

REFERENCES

Dejoan, A., and Leschziner, M. A., 2004a, "Large eddy simulation of a plane turbulent wall jet", *Phys. Fluids*, to appear.

Dejoan, A., and Leschziner, M. A., 2004b, "LES study of the statistical characteristics of the plane turbulent wall jet", *Proceedings of the Tenth European Turbulence Conference, H.I Andersson and P.-A. Krögstad (Eds)*, pp. 663–666.

Dejoan, A., and Leschziner, M. A., 2005, "Assessment of turbulence models for predicting the interaction region in a wall jet by reference to LES solution and budgets", *ETMM6, Sardinia, Italy.*

Eriksson, J. G., Karlsson, R. I., and Persson, J., 1998, "An experimental study of a two-dimensional plane turbulent wall jet", *Experiments in Fluids*, Vol. 25, pp. 50-60.

Germano, M., Piomelli, U., Moin, P., and Cabot, W., 1991, "Dynamic subgrid-scale eddy viscosity model", *Phys. Fluids A*, Vol. 3 pp. 1760-1765.